The impact of high frequency rapid viral antigen screening on COVID-19 spread and outcomes: a validation and modeling study

Authors: Beatrice Nash[1,2*], Anthony Badea[1,3*], Ankita Reddy[1,4*], Miguel Bosch[1,5], Nol Salcedo[1], Adam R. Gomez[1], Alice Versiani[6], Gislaine Celestino Dutra Silva[6], Thayza Maria Izabel Lopes dos Santos[6], Bruno H. G. A. Milhim[6], Marilia M Moraes[6], Guilherme Rodrigues Fernandes Campos[6], Flávia Quieroz[6], Andreia Francesli Negri Reis[6], Mauricio L. Nogueira[6], Elena N. Naumova[7], Irene Bosch[1,8], Bobby Brooke Herrera[1,9†]

[*]These authors contributed equally to this work.

Affiliations:

[1]E25Bio, Inc., Cambridge, MA, USA

[2]Department of Computer Science, Harvard University School of Engineering and Applied Sciences, Cambridge, MA, USA

[3]Department of Physics, Harvard University, Cambridge, MA, USA

[4]Perelman School of Medicine, University of Pennsylvania, Philadelphia, PA, USA

[5]InfoGeosciences LLC, Houston, TX, USA

[6]Faculdade de Medicina de São José do Rio Preto (FAMERP), São José do Rio Preto, Brazil

[7]Division of the Nutrition Epidemiology and Data Science, Friedman School of Nutrition Science and Policy, Tufts University, Boston, MA, USA

[8]Department of Medicine, Mount Sinai School of Medicine, New York, NY, USA

[9]Department of Immunology and Infectious Diseases, Harvard T.H. Chan School of Public Health, Boston, MA, USA

†Corresponding Author. BBH, email: bbherrera@e25bio.com

Abstract

High frequency screening of populations has been proposed as a strategy in facilitating control of the COVID-19 pandemic. Here we use computational modeling, coupled with clinical data from a rapid antigen test, to predict the impact of frequent rapid testing on COVID-19 spread and outcomes. Using patient nasopharyngeal or nasal swab specimens, we demonstrate that the sensitivity/specificity of two rapid antigen tests compared to quantitative real-time polymerase chain reaction (qRT-PCR) are 80.0%/91.1% and 84.7%/85.7%, respectively; moreover, sensitivity correlates directly with viral load. Based on COVID-19 data from three regions in the United States and São José do Rio Preto, Brazil, we show that high frequency, strategic population-wide rapid testing, even at varied accuracy levels, diminishes COVID-19 infections, hospitalizations, and deaths at a fraction of the cost of nucleic acid detection via qRT-PCR. We propose large-scale antigen-based surveillance as a viable strategy to control SARS-CoV-2 spread and to enable societal re-opening.

INTRODUCTION

The COVID-19 pandemic has taken an unprecedented toll on lives, wellbeing, healthcare systems, and global economies. As of 25 September 2020, there have been more than 32.1 million confirmed cases globally with more than 980,000 confirmed deaths (*1*). However, these numbers and the current mapping of disease spread present an incomplete picture of the outbreak largely due to the lack of adequate testing, particularly as undetected infected cases are the main source of disease spread (*2–7*). It is estimated that the reported detection rate of actual COVID-19 cases is only 1-2% (*5*). As of September 2020, the United States and Brazil remain the top two countries with the highest number of COVID-19 cases and deaths worldwide. As countries begin to re-open their economies, a method for accessible and frequent surveillance of COVID-19, with the necessary rapid quarantine measures, is crucial to prevent the multiple resurgences of the disease.

The current standard of care rightfully places a strong focus on the diagnostic limit of detection, yet frequently at the expense of both cost and turnaround time. This situation has contributed to limited population testing largely due to a dearth of diagnostic resources. Quantitative real-time polymerase chain reaction (qRT-PCR) is the gold-standard method for clinical diagnosis, with high sensitivity and specificity, but these tests are accompanied by the need for trained personnel, expensive reagents and instrumentation, and a significant amount of time to execute. Facilities offering qRT-PCR sometimes require a week or longer to complete and return the results to the patient. During this waiting period the undiagnosed individual may spread the infection and/or receive delayed medical treatment. Moreover, due to the cost and relative inaccessibility of qRT-PCR in both resource-limited and abundant settings, large-scale screening using qRT-PCR at frequent intervals remains impractical to identify infected but asymptomatic or mildly symptomatic infections. Numerous studies have reported asymptomatic COVID-19 cases

as well as a variation in viral load within and between individuals at different time points, suggesting the need for more frequent testing for informative surveillance.

Technologies alternate to qRT-PCR, such as rapid viral antigen detection, clustered regularly interspaced short palindromic repeats (CRISPR), and loop-mediated isothermal amplification (LAMP) of SARS-CoV-2 provide potential large-scale screening applications, yet their implementation is stymied by requirements for qRT-PCR-like accuracy before they can reach the market (*8*). In countries such as India, where the qRT-PCR resources would not be sufficient to cover monitoring of the population, the use of rapid antigen tests is well underway(*9*, *10*). In early May 2020, the United States Food and Drug Administration (FDA) authorized the first antigen test for the laboratory detection of COVID-19, citing a need for testing beyond molecular and serological methods. Antigen testing detects the viral proteins rather than nucleic acids or human antibodies, allowing for detection of an active infection with relative ease of sample collection and assay. These rapid assays – like other commercially-available rapid antigen tests - can be mass-produced at low prices and be administered by the average person without a laboratory or instrumentation. These tests also take as little as 15 minutes to determine the result, enabling real-time surveillance and/or diagnosis. Although antigen tests usually perform with high specificities (true negative rate), their sensitivity (true positive rate) is often lower when compared to molecular assays. While qRT-PCR can reach a limit of detection as low as 10^2 genome copies per mL, rapid antigen testing detects viral protein that is assumed to correlate with approximately 10^5 genome copies per mL (*11*).

We hypothesize that frequent antigen-based rapid testing even with lower sensitivities compared to qRT-PCR - along with appropriate quarantine measures - can be more effective at decreasing COVID-19 spread than less frequent molecular testing of symptomatic individuals.

Keeping in mind the realities of daily testing in resource-limited regions, we also hypothesize that testing frequency can be adjusted according to the prevalence of the disease; that is, an uptick in reported cases should be accompanied by more frequent testing. During the viral incubation period, high infectivity correlates with a high viral load that can be detected by either qRT-PCR or rapid antigen testing (*12–16*). Rapid tests thus optimize diagnosis for the most infectious individuals. Studies also point to the relatively small window of time during an individual's incubation period in which the qRT-PCR assay is more sensitive than rapid tests (*12*).

In this study we report the clinical validation of two direct antigen rapid tests for detection of SARS-CoV-2 spike glycoprotein (S) or nucleocapsid protein (N) using retrospectively collected nasopharyngeal or nasal swab specimens. Using the clinical performance data, we develop a modeling system to evaluate the impact of frequent rapid testing on COVID-19 spread and outcomes using a variation of a SIR model, which has been previously used to model COVID-19 transmission (*17–23*). We build on this model to incorporate quarantine states and testing protocols to examine the effects of different testing regimes. This model distinguishes between undetected and detected infections and separates severe cases, specifically, those requiring hospitalization, from those less so, which is important for disease response systems such as intensive care unit triaging. We simulate COVID-19 spread with rapid testing and model disease outcomes in three regions in the United States and São José do Rio Preto, Brazil - the site of the clinical validation study - using publicly available data. To date, COVID-19 modeling describes the course of disease spread in response to social distancing and quarantine measures, and a previous simulation study has shown that frequent testing with accuracies less than qRT-PCR, coupled with quarantine process and social distancing, are predicted to significantly decrease infections (*12*, *17*, *23–27*). This is the first modeling system using publicly-available data to simulate how potential public

health strategies based on testing performance, frequency, and geography impact the course of COVID-19 spread and outcomes. Our findings suggest that a rapid test, even with sensitivities lower than molecular tests, when strategically administered 2-3 times per week, will reduce COVID-19 spread, hospitalizations, and deaths at a fraction of the cost of nucleic acid testing via qRT-PCR. Modern surveillance systems should be well equipped with rapid testing tools to ensure that disease tracking and control protocols are effective and well-tailored to national, regional, and community needs.

RESULTS

Accuracy of Direct Antigen Rapid Tests Correlate with Viral Load Levels

Rapid antigen tests have recently been considered a viable source for first-line screening, although concerns about the accuracy of these tests persist. We clinically validated two different direct antigen rapid tests for the detection of either N or S from SARS-CoV-2 in retrospectively collected nasal or nasopharyngeal swab specimens. Of the total number of nasal swab specimens evaluated by qRT-PCR for amplification of SARS-CoV-2 N, S, and ORF1ab genes, 100 tested positive and 90 tested negative (Table 1, Table S1). The overall sensitivity and specificity of the rapid antigen test for detection of SARS-CoV-2 N, evaluated across the nasal swab specimens, was 80.0% and 91.1%, respectively. Of the total number of nasopharyngeal swab specimens evaluated by qRT-PCR for amplification of SARS-CoV-2 N, RNA-dependent RNA polymerase (RdRp), and envelope (E) genes, 72 tested positive and 49 tested negative (Table 2, Table S1). The overall sensitivity and specificity of the rapid antigen test for detection of SARS-CoV-2 S, evaluated across the nasopharyngeal swab specimens was 84.7% and 85.7%, respectively.

Altogether, our data demonstrate that the sensitivity of the rapid antigen tests are positively correlated to the viral load level (Table S1).

The Ct value indirectly quantifies the viral RNA copy number related to the viral load of the sample for the specific assay (*28*, *29*). Ct values represent the number of qRT-PCR cycles at which generated fluorescence crosses a threshold during the linear amplification phase; Ct values are therefore inversely related to the viral load. Notably, the sensitivity of both rapid antigen tests increases as Ct value decreases (Table S1). The sensitivity of the rapid antigen test for detection of SARS-CoV-2 N increased from 80.0% at Ct values <40 to 95.8% at Ct values <20. Similarly, the sensitivity of the rapid antigen test for detection of SARS-CoV-2 S increased from 84.7% at Ct values <35 to 100.0% at Ct values <15. Taken together, the clinical data shows that the rapid antigen test performs with increasing accuracy for individuals with a higher viral load, and potentially the most infectious (*13–16*).

An Enhanced Epidemiological SIDHRE-Q Model

We propose an enhanced epidemiological modeling system, *SIDHRE-Q,* a variant of the classical SIR model in order to expand our clinical validation study and to understand the effects of using frequent rapid tests such as the rapid antigen test on COVID-19 outbreak dynamics. The changes we make to the basic model to encompass the unique characteristics of the COVID-19 pandemic are similar to those presented by Giordano et al. *(16)* (Figure 1, Figure S1). The differential equations governing the evolution of the *SIDHRE-Q* model and descriptions of the parameter values are provided in the material and methods section (Equation 2, Table 3).

An individual that begins in **S** may either transition to a Quarantine Uninfected (**Q-U**) state via a false positive result or to an Infected Undetected (**I**) state via interaction with an infected

individual. Should an individual in **S** move into **Q-U**, they are quarantined for 14 days before returning to **S**, a time period chosen based on current knowledge of the infectious period of the disease. One could also conceive of an effective strategy in which individuals exit quarantine after producing a certain number of negative rapid tests in the days following their initial positive result or confirm their negative result using qRT-PCR.

Given that those diagnosed are predominantly quarantined, individuals in **I** interact more with the **S** population than do those in Infected Detected (**D**). Therefore, the infectious rate for **I** is assumed to be significantly larger than for **D**. Furthermore, a region's ability to control an outbreak is directly related to how quickly and effectively people in **I** test into **D**, reducing their infectiousness through quarantine. This study, in particular, highlights the critical role frequency of testing, along with strict quarantine, has in mitigating the spread of the disease and provides specific testing strategies based on rapid tests we predict to be highly effective.

In this model, we assume that individuals receive a positive diagnosis before developing severe symptoms and that those with symptoms severe enough to be potentially fatal will go to the hospital. If an individual develops symptoms, we assume they are tested daily until receiving a positive result; hence, before severe symptoms develop, they will be diagnosed with high probability. Those who do not develop symptoms are tested according to the frequency of tests administered to the general population. Therefore, there is no modeled connection between **I** and **H** or between **I** and **E**. Removing these assumptions would have negligible impact on the results as these flows are very small.

Should an individual test positive and transition to **D**, they may either develop serious symptoms requiring care or recover. Those who develop serious symptoms and transition to state **H** will then transition to either **R** or **E**. The recovered population is inevitably tested, as infected

206 individuals may recover without being detected. Therefore, the Quarantined Recovered (**Q-R**)
207 state is introduced with the same connections to **R** as the connections between **S** and **Q-U**. Though
208 the reinfection rate of SARS-CoV-2 has been a point of recent debate, it is assumed that the number
209 of re-infected individuals is small (*30–34*). Therefore, individuals cannot transition from **R** to **S**,
210 hence the separately categorized quarantined populations.

211 We considered several variations and extensions of the *SIDHRE-Q* model. In simulations,
212 we tested additional states, such as those in the *SIDARTHE* model, which include distinctions
213 between symptomatic and asymptomatic cases for both detected and undetected populations (*17*).
214 Incorporating information about the correlations between viral load and infectivity and sensitivity
215 were also considered. Altogether, our modeling system has been well tuned to predict the impact
216 of high frequency rapid testing on COVID-19 spread and outcomes.

217

218 **Frequent Rapid Testing with Actionable Quarantining Dramatically Reduces Disease**
219 **Spread**

220 In order to demonstrate how strategies could affect the disease spread in different
221 geographies and demographics, we used surveillance data obtained from regions of varying
222 characteristics: the state of Massachusetts (MA), New York City (NYC), Los Angeles (LA), and
223 São José do Rio Preto (SJRP), Brazil, the site of the rapid antigen test clinical validation study.
224 These regions are also selected in our study due to the readily available surveillance data provided
225 by the local governments. We fit the model to the data from each region starting 1 April 2020. At
226 this time point the disease reportedly is most advanced in NYC and least advanced in SJRP, Brazil
227 with estimated cumulative infection rates of 7.11% and 0.12%, respectively.

After calibrating the *SIDHRE-Q* model, the disease spread is observed with varying validated rapid antigen test performances and frequencies (Figure 2A). Sensitivity (the ratio of true positives to the total number of positives) and specificity (the ratio of true negatives to the total number of negatives) compared to gold-standard qRT-PCR were used as measures of test accuracy.

The rapid test frequency is varied while maintaining an accuracy of 80% sensitivity and 90% specificity, comparable to our clinical data collected in SJRP, Brazil. These testing scenarios are then compared to symptomatic testing, in which individuals receive a rapid test only when presenting symptoms, via either a rapid test or qRT-PCR. Since the primary testing regiment deployed in MA, LA, NYC and SJRP, Brazil is qRT-PCR-based and focused on symptomatic individuals, the symptomatic testing protocol via qRT-PCR is directly estimated from the data to be the rate ν (Table 3).

The difference between the qRT-PCR and rapid test simulations (red and orange lines, respectively) is therefore only sensitivity of testing (Figure 2A). We assumed that test outcome probability is a function only of whether an individual is infected and independent of other factors; one can consider this a lower bound on effectiveness of a strategy, as sensitivity and infectivity are often positively correlated with antigen testing.

To better understand the effect of rapid testing frequency and performance on healthcare capacity and mortality rates, we simulate the testing strategy with 30%-90% sensitivity each with 80% or 90% specificity against the symptomatic testing strategy (Figure S2).

As per our hypothesis, frequency and symptom-based testing dramatically reduced infections, simultaneous hospitalizations, and total deaths when compared to the purely symptom-based testing regiments, and infections, hospitalization, and death were reduced as frequency

increased. Although testing every day was clearly most effective, even testing every fourteen days with an imperfect test gave an improvement over symptomatic testing with qRT-PCR. While the strategy works best when implemented at the very beginning of an outbreak, as demonstrated by the results in SJRP, Brazil, it also works to curb an outbreak that is already large, as demonstrated by the results in NYC. The difference between frequencies is more noticeable when the testing strategy is applied to the outbreak in NYC, leading us to hypothesize that smaller outbreaks require a lower testing frequency than larger ones; note the difference between the dependence on frequency to curb a small initial outbreak in SJRP, Brazil versus a large one in NYC (Figure 2B).

For test performance of 80% sensitivity and 90% specificity, the percent of the population that has been infected in total from the beginning of the outbreak to mid-July drops from 18% (MA), 11% (LA), 26% (NYC), and 11% (SJRP, Brazil) to 3%, 2%, 12%, and 0.26%, respectively, using a weekly rapid testing and quarantine strategy (with regards to predictions of overall infection rates, other studies based on seroprevalence and epidemiological predictions have reached similar conclusions (*35*, *36*)). If testing is increased to once every three days, these numbers drop further to 1.6% (MA), 1.4% (LA), 9.4% (NYC), and 0.19% (SJRP, Brazil) (Table S2).

To further examine the relationship between frequency and sensitivity, we modeled the maximum number of individuals in a given state over the 105-day time period for four geographic regions (Figure 2B, Figure S3). In all four geographic regions, as frequency of testing increases, the total infections, maximum simultaneous hospitalizations, and total deaths converge to small percentages regardless of the sensitivity at high frequencies. It is clear that the difference in frequency required to achieve the same result using tests of differing sensitivities is very small. For example, we predict that for the outbreak in LA, a testing strategy started on 1 April of every

10 days using a test of sensitivity 90% would have resulted in 2.5% of the population having been infected, while using a test of sensitivity 30% would require a strategy of every 5 days to achieve the same number. Thus, we conclude that frequency is more important than sensitivity in curbing the spread, and a large range of sensitivities prove effective when testing sufficiently often (Figure S3). How frequently, exactly, depends on the specific outbreak and what stage it is in, which leads us to the location-based deployment strategy discussed in a later section. Frequency of testing can be significantly reduced to effectively contain the disease once the initial outbreak has been controlled; it is clear that this takes only a matter of weeks (Figure 2A).

On the other hand, according to the specificity of the rapid test and the quarantine duration, larger testing frequency result in a larger percent of the population quarantined (Figure 2A). Assuming a 90% rapid test specificity and 14-day quarantine duration, for the 1-, 3- and 7-day frequencies almost 60%, 38% and 20% of the population, respectively, would be quarantined. This figure may be reduced with additional rules for exiting quarantine early, such as after complementary testing. An example of such a strategy is that individuals who test positive are required to either quarantine for two weeks or produce two consecutive negative rapid tests in the two days following their positive result. Assuming 80% sensitivity and 90% specificity, those individuals will reenter the public while still infected with probability 0.04. If uninfected, that individual will exit quarantine after two days with probability 0.81. However, a compromise between the reduction of infections and the proportion of the population in quarantine would be part of the planning for the appropriate testing protocol in each community or region.

Additionally, while high frequency may be necessary to contain a large outbreak initially, relatively infrequent testing, such as every one or two weeks, is sufficient to keep controlled

outbreaks small, while reducing the number of quarantined individuals to less than 10% of the population using a two-week mandatory quarantine.

A County-Based Testing Strategy Offers a Cost-effective Approach to Large-scale COVID-19 Surveillance

To examine the effects of resource-strategic testing schemes, we modeled the COVID-19 prevalence by varying testing frequency across counties of California. For this analysis, only California was analyzed because of the accessibility of the county level data. In this scheme, the percent of active infected detected individuals in a county determines the frequency of testing. We define thresholds for the number of active detected infections that, when hit, initiate testing protocols of different frequencies depending on the threshold hit. We first tested evenly spaced thresholds for the number of detected active infections up to 1% of the population, but later adopted thresholds that were determined according to Equation 1. In Equation 1, D = population of state **D** at the time of testing. T = number of active infections which, if reached, initiates everyday testing. The days between tests are rounded to the closest integer value.

$$\text{Days between tests} = \max\left(1, 2\log_2(T/D) + 1\right) \quad (1)$$

The days between tests are chosen such that the detected active infections should remain near to or below T. If the initial detected active infections are greater than T, then the testing frequency of 1 will cause infections to rapidly drop. Both the threshold at which everyday testing begins and the coefficient of $log_2 T/D$ can be modified to produce a strategy that is more or less frequent in testing or resource effective; a range of days between tests from 14 days to 1 day are used (Figure 3). A scan over different choices of T is shown in Figures S5 and S6; the threshold

we choose in Figure 3 is 0.05% because it is successful in curbing the outbreak within the time period we consider. While these choices work for the epidemic in California at the point we start our simulations, 10 April, they do not necessarily reflect the most resource effective choices everywhere. Our analysis could be redone to select the best strategy in other states or in the country as a whole.

Using a rapid test with a sensitivity of 80% and specificity of 90%, the county-based testing with threshold 0.05% reduces the active infections from 0.94% to 0.0005%, while the uniform strategy with tests administered every 7 days results in double the number of active infections (Figure 3). As the threshold is reduced, the total cost increases while the cumulative infections, maximum percentage hospitalized, and cumulative deaths all decrease (Figure S4).

Strategy B in Figure 3 consists of qRT-PCR testing uniformly applied to the highlighted population with a frequency of once weekly. The average cost per person per day is just under $15. Despite this frequency and the accuracy of qRT-PCR, the strategy does not succeed in curbing the spread as fast as strategy A, which uses a testing sensitivity and specificity of 80% and 90%, respectively, and testing frequency that vary between counties depending on the proportion of their population that is currently infected. The total cost for strategy A is estimated at a fraction of the other at $1.53 per person per day.

DISCUSSION

In this study we examine the potential effects of a novel testing strategy to limit the spread of SARS-CoV-2 utilizing rapid antigen test screening approaches. Our clinical data and *SIDHRE-Q* modeling system demonstrate that 1) frequent rapid testing even at a range of accuracies is effective at reducing COVID-19 spread, 2) rapid antigen tests are a viable source for this strategy

and diagnose the most infectious individuals, and 3) strategic geographic-based testing can optimize disease control with the amount of available resources. The information from a diagnostic test itself is of tremendous value, as it can prompt the necessary quarantine measures to prevent spread, guide proper care and triage, and provide crucial disease-tracking information. Diagnostic testing in the United States and abroad, however, has been a significant public health hurdle. The public has witnessed and experienced symptomatic individuals being denied testing due to shortages, and few testing structures for asymptomatic or mildly symptomatic individuals – a significant source of disease spread. Though several factors contributed to the stymied early response measures, such as lockdown and quarantine protocols and adherence, severe testing bottlenecks were a significant culprit (*37–39*). Early control measures have been shown to decrease lives lost by several orders of magnitude (*40*). These challenges, though exacerbated during the early months of the pandemic, remain at the forefront of the public health crises.

Diagnosis of SARS-CoV-2 infection by qRT-PCR is the current standard of care, yet remains expensive and requires a laboratory and experienced personnel for sample preparations and experimentation. Significantly, the turnaround time for results can be up to 10 days (*41*). On an individual scale, this leaves the public in limbo, preventing people from either leaving quarantine if they are negative, or delaying critical care and infecting others if they are positive. On a societal level, this current testing scheme yields incomplete surveillance data on which response efforts such as societal reopening and hospital management depend. Though qRT-PCR is considered the gold-standard diagnostic method because of its high sensitivity and specificity, the logistical hurdles render it unrealistic for large-scale screening.

As qRT-PCR remains impractical for this strategy, and rapid tests are facing regulatory challenges because they do not perform with qRT-PCR-like accuracy, rapid test screening is either

366 nonexistent in several countries or symptom-based. Even under best-case assumptions, findings
367 have shown that symptom and risk-based screening strategies miss more than half of the infected
368 individuals (*42*). Some have argued that the need for widespread testing is overstated due to the
369 variability in test sensitivity and specificity (*43*). Here, we present alternative large-scale
370 diagnostic tools to qRT-PCR, and show that test performance, though valuable, is secondary to
371 widespread test frequency, which is enabled by accessibility and turnaround time. Furthermore,
372 test affordability is essential for the successful implementation in communities most affected by
373 infection and will to speed up the safe opening and functioning of the viral sectors of the economy.
374 Giordano et al. has modeled the evolution of SARS-CoV-2 spread, introducing a diagnosed
375 state to elucidate the importance of population-wide testing (*17*). Mina et al. has examined how
376 various test sensitivities and frequencies affect the reproductive number (*12*). We build upon these
377 findings to show how in affected United States and Brazil regions, population-wide frequent and
378 rapid testing schemes, with sensitivities ranging from 30%-90%, can be more effective in curbing
379 the pandemic than a PCR-based scheme. Integrating real-world surveillance and clinical data into
380 our modeling system has allowed us to incorporate regional differences - such as variances in
381 healthcare access, state health policy and adherence, state GDP, and environmental factors - under
382 the same model. Significantly, our findings hold true across Massachusetts, New York City, Los
383 Angeles, and São José do Rio Preto, Brazil. We also present the economic considerations of these
384 testing regimes, showing that widespread rapid testing is more cost efficient than less frequent
385 qRT-PCR testing. In line with these economic considerations, our model demonstrates the
386 effectiveness of a geographic-based frequent testing regime, in which high disease prevalence
387 areas receive more frequent testing than low disease prevalence areas.

Since COVID-19 is known to affect certain demographics differently, modeling would benefit from incorporating demographic information correlated with disease progression and spread to define sub-models and sets of parameters accordingly. Age, pre-existing conditions, job types, and density of population are examples of possible categories, each of which influence the risk of contracting and/or dying from COVID-19. Further studies would benefit from incorporating these ideas to better understand the effectiveness of rapid testing on identifying potential super spreading events. Future public health prevention programs should use the proposed modeling system to develop and test scenarios for precision testing and prevention.

Our findings also point to low-cost tools for implementation of this testing strategy, such as a rapid antigen-based test for the detection of SARS-CoV-2 proteins. We show that the rapid antigen tests perform with a range of accuracies under which disease spread can be dramatically mitigated under our model. Notably, the sensitivity is correlated to the individual's viral load, effectively diagnosing those who are potentially the most infectious with the highest accuracy. Our findings are significant because rapid antigen tests are cheaper than qRT-PCR, can be mass produced to millions per day, present results within 15 minutes, and can be administered by a nonexpert without a lab or special equipment.

There are several policy implications for these findings. First, our model supports that systems of high frequency rapid testing should be implemented as a first-line screening method. This can be first enabled by a more holistic regulatory evaluation of rapid diagnostics, such that policy emphasizes accessibility and turnaround time even under a range of accuracies. One can imagine a less accurate, though rapid method of first-line screening in schools, public transportation, and airports, or even at home, and a qRT-PCR-based method for second-line screening (testing those who present severe symptoms or have been in contact with infected

411 individuals, testing in a clinical setting, etc). Second, our cost analysis and rapid antigen test data
412 present a viable and potentially more cost-effective method for screening. Third, our county-based
413 testing scheme presents a possible method for wide-scale screening while optimizing resources.
414 Future studies should investigate how this selective testing strategy can be applied to different
415 location scales to further inform health policy. Moreover, though our models analyze regions in
416 the United States and Brazil, similar testing strategies can be considered globally in both resource
417 limited and abundant settings due to the higher accessibility of rapid tests compared to qRT-PCR.

418 We emphasize that integral to the effectiveness of diagnostic schemes is 1) the proper
419 adherence to quarantine measures and 2) the combined use of a variety of diagnostic methods
420 including nucleic acid, antigen, and antibody tests. According to these models, rapid antigen tests
421 are an ideal tool for first-line screening. Clinical molecular tests such as qRT-PCR are vital to the
422 diagnostic landscape, particularly to re-test suspected cases that were negative on the rapid test.
423 Because rapid tests present a higher rate of false negatives, methods such as qRT-PCR remain
424 integral to second-line screening. Antibody tests provide important information for immunity and
425 vaccination purposes as well as epidemiological surveillance. This model also assumes that
426 individuals will quarantine themselves before being tested and for 14 days following a positive
427 diagnostic result.

428 Our simulations combined with real-world data demonstrate a robust modeling system and
429 elucidates the significance of this novel testing strategy. However, there are important limitations
430 to be considered. Differences in disease reporting between the geographical regions and the
431 incomplete nature of COVID-19 surveillance data, often due to the lack of testing, are not
432 considered in the model. It is imperative that the testing results, hospitalization and death statistics,
433 and changes in protocol are reported in real-time to scientists and policy makers so that models

can be accurately tuned as the pandemic develops. The model also does not take into account infrastructural limitations such as hospital capacity. Though the rapid antigen test offers several advantages such as affordability, fast turnaround time, and ease of mass production, we are also assuming that there are systems in place to implement frequent and safe low-cost screening across different communities and settings.

Our model underscores the need for a point-of-care or at-home test for frequent screening, particularly as lockdown restrictions ease. Regulatory agencies such as the FDA could work towards regulating rapid tests to alternative standards other than comparison to high sensitivity molecular diagnostics, as our model shows that frequency and scale of testing may overcome lower sensitivities. Rather, we could refocus policy to implement first-line screening that optimizes accuracy with efficiency and equitability.

MATERIAL AND METHODS

Development of Direct Antigen Rapid Tests for the Detection of SARS-CoV-2

We developed a direct antigen rapid test for the detection of the nucleocapsid protein or spike glycoprotein from SARS-CoV-2 in nasal or nasopharyngeal swab specimens as previously described (*44*). Briefly, the rapid antigen tests are immunochromatographic format with a visual readout using anti-N or anti-S mouse monoclonal antibodies (E25Bio, Inc., Cambridge, MA, USA) that are either coupled to 40 nm gold nanoparticles (Abcam, Cambridge, UK) or adsorbed to nitrocellulose membranes (Sartorius, Goettingen, Germany). Each rapid antigen test has a control area adjacent to the paper absorbent pad; the control is an anti-mouse Fc domain antibody (Leinco Technologies, Fenton, MO, USA) that will capture any of the antibody-conjugated gold nanoparticles to generate a control visual signal. A visual signal at the test area reflects SARS-

457 CoV-2 N or S that is "sandwiched" between an anti-N or anti-S antibody adsorbed to the
458 nitrocellulose membrane and a second anti-N or anti-S antibody covalently coupled to visible gold
459 nanoparticles.
460
461 **Validation of Direct Antigen Rapid Test for the Detection of SARS-CoV-2**
462 In a retrospective study of nasal swab specimens form human patients, we compared the
463 accuracy of the rapid antigen test for detection of SARS-CoV-2 N to the viral loads of individuals.
464 Nasal swab specimens (n=190) were tested following approved human subjects use protocols. The
465 nasal swab specimens were banked frozen from suspected patients submitted to PATH for routine
466 COVID diagnosis. Prior to using the rapid test, the nasal swab specimens were validated by qRT-
467 PCR using the FDA EUA ThermoFisher/AppliedBiosystems TaqPATH COVID-19 Combo Kit
468 (ThermoFisher, Waltham, MA USA). The primary study under which the samples and data were
469 collected received ethical clearance from the PATH Research Ethics Committee, protocol number
470 00004244. The nasal swab specimens were de-identified, containing no demographic data, prior
471 to analysis.
472 Additionally, in a retrospective study of nasopharyngeal swab specimens from human
473 patients, we compared the accuracy of the rapid antigen test to the viral load of individuals.
474 Nasopharyngeal swab specimens (n = 121) were tested in Brazil following approved human
475 subjects use protocols. The age of study participants ranged from 1 to 95 years with an overall
476 median of 37 years (interquartile range, 27–51 years), and 62% were female. The demographic
477 summary of the patients are included in Table S3. The nasopharyngeal swab specimens were
478 banked refrigerated or frozen samples from suspected patients submitted to the lab for routine
479 COVID diagnosis. Prior to using the rapid test, the nasopharyngeal swab samples were validated

by qRT-PCR using GeneFinder™ COVID-19 Plus Real*Amp* Kit (OSANGHealtcare, Anyang-si, Gyeonggi-do, Republic of Korea I). The primary study under which the samples and data were collected received ethical clearance from the Faculdade de Medicina de São José do Rio Preto (FAMERP), protocol number 31588920.0.0000.5415. All excess samples and corresponding data were banked and de-identified prior to the analyses.

A nasopharyngeal swab specimen (1 mL) was concentrated using a Vivaspin 500 centrifugal concentrator (Sartorius, Goettingen, Germany) at 12,000 x g for 10 minutes. The concentrated nasopharyngeal swab specimen retentate was transferred to a collection tube and the rapid antigen test was inserted into the tube with the retentate and allowed to react for 15 minutes. After processing of the rapid antigen test, the visual positive or negative signal was documented.

Data for Modeling

As of August 2020, the United States and Brazil have the highest number of confirmed COVID-19 cases and deaths worldwide, with both countries reporting their first case on 26 February 202) (*1*). Although several affected US regions could have been modeled, we look at data from Massachusetts, New York, and Los Angeles: these regions each contained “hotspots”, or areas of surging COVID-19 cases, at different points in time during the pandemic and have publicly available government-provided surveillance data. Our model is fit using data over 105 days beginning on April 1 for Figure 2 and 105 days beginning on April 10 for Figure 3 (see “Modeling Parameters” in Methods). In order to understand the various testing proposals on a global scale, we performed our clinical study in and expanded the modeling study to Brazil. The specific data we use to fit our model are cumulative confirmed cases, total deaths, and number of

daily hospitalizations due to COVID-19. This surveillance data was retrieved from government-provided online databases (*45–51*).

Modeling Parameters

Equation 2 below provides the exact differential equations governing the model.

$$
\begin{aligned}
\mathrm{d}\mathbf{S} &= &&-\mathbf{S}\left(\alpha\mathbf{I}+\eta\mathbf{D}+\gamma\right) &&+\psi\mathbf{Q_U}\\
\mathrm{d}\mathbf{I} &= &&-\mathbf{I}\left(\varepsilon+\lambda+\nu\right) &&+\mathbf{S}\left(\alpha\mathbf{I}+\eta\mathbf{D}\right)\\
\mathrm{d}\mathbf{D} &= &&-\mathbf{D}\left(\frac{\mathbf{D}+\mathbf{I}}{\mathbf{D}}\mu+\rho\right) &&+\mathbf{I}(\nu+\varepsilon)\\
\mathrm{d}\mathbf{H} &= &&-\mathbf{H}\left(\sigma+\tau\right) &&+\mu\left(\mathbf{D}+\mathbf{I}\right)\\
\mathrm{d}\mathbf{E} &= &&&&+\tau\mathbf{H}\\
\mathrm{d}\mathbf{R} &= &&-\gamma\mathbf{R} &&+\rho\mathbf{D}+\lambda\mathbf{I}+\sigma\mathbf{H}+\psi\mathbf{Q_R}\\
\mathrm{d}\mathbf{Q_U} &= &&-\psi\mathbf{Q_U} &&+\gamma\mathbf{S}\\
\mathrm{d}\mathbf{Q_R} &= &&-\psi\mathbf{Q_R} &&+\gamma\mathbf{R}
\end{aligned}
\qquad (2)
$$

In order to determine the values of the parameters defining the flows between states, we use a least squares regression performed at seven day intervals in the datasets to which we fit. This allows the model to take into account the time dependent nature of the parameters, which rely on factors such as social distancing regulations and changes in testing capacity. We also fit window sizes between 1 and 21 days and find that while the fit degrades with larger window size, the overall shape of the fits do not change. We choose seven days assuming policy changes take a week to become effective and that reasonable parameters can be expected to change within this time period. Also, the seven day window size accounts for the fact that often data is not reported as diligently over the weekend. Time series of the values of the parameters for the geographic locations discussed in this paper are included in Figure S5.

Given the restrictions on data available for the populations of various states, varying all of the parameters results in an over parameterized system. Therefore, a subset of the model parameters are fit while the others are either extracted from other sources; see Table 3.

The fitting procedure minimizes the sum of the squared residuals of the total cases, current daily hospitalizations, cumulative deaths, and percentage of total infected individuals currently hospitalized. The first three are present in the data sets while the latter is derived from the estimates of the ratio between infected undetected to infected detected individuals from the CDC Laboratory Seroprevalence Survey Data (*52*). While this ratio changes over time, the percentage of infected individuals developing severe symptoms should remain roughly constant throughout the course of the epidemic in the different locations studied.

We consider the data sets for outbreaks in MA, NYC, LA, and SJRP, Brazil (*45–50*). While each location has testing and fatality information dating back to January, hospitalization data was not included until late March (for NYC and SJRP) and April (for MA and LA). Hence we begin our fitting procedure and testing strategy on 1 April for each of the data sets; by this point, the outbreak is advanced in NYC, substantial in MA, non-negligible, but far from its peak, in LA, and in early stages in SJRP, Brazil. Starting simulations at various stages of the outbreak allows one to see the difference in results between when a testing strategy is administered.

In order to determine the effectiveness of the county-based strategy when applied to the state of California, we also fit all of the counties in California with a population greater than 1.5% of that of the entire state and with greater than zero deaths. The results do not depend on these selections, but instead suggest a practical criteria to administer limited resources. The fitting is done starting 10 April for these counties, as at this point the outbreak is sufficiently well-

541 documented in each to successfully model. For the county-level data we compute a seven day
542 running average of each of the data sets to which we then fit in order to smooth out fluctuations in
543 the data, likely due to reporting, which are more significant here than in the other data sets
544 considered, as the county populations are smaller and hence discrepancies impact the smoothness
545 of the data more. The fits for each of the counties can be found in Figure S6.

546 As one can see from Figure 1, these data sets are particularly not smooth, which indicates
547 inefficiencies in reporting. Additionally, it is difficult to gauge their consistency within the dates
548 provided or to compare between locations, as reporting mechanisms changed over time within the
549 same locations. Despite this lack of consistency, our model and fitting mechanism was successful
550 in reproducing the progress of the outbreak in each data set studied.

551 The authors confirm that the data supporting the findings of this study are available within the
552 article and/or its supplementary materials; any other data will be made available upon request. Our
553 code can be found on github: https://github.com/badeaa3/COVID19_Rapid_Testing. The code is
554 written using python with the packages scipy, numpy, lmfit, matplotlib and plotly (*53–57*).

555

556

557

558

559

560

561

562

563

H2: Supplementary Materials

Results

Table S1. Data summary of direct antigen rapid test (DART) for detection of SARS-CoV-2 nucleocapsid protein and DART for detection of SARS-CoV-2 spike glycoprotein performance in comparison to qRT-PCR results.

Table S2. Summary of results of COVID-19 outcomes in 3 US Regions and Brazil as a result of Frequent Rapid Testing Protocol using SIDHRE-Q Model. Total Infected, Maximum Hospitalized, and Total Deaths are shown for Massachusetts, Los Angeles, New York, and São Jose do Rio Preto, Brazil under a qRT-PCR protocol (symptomatic testing) and a Rapid Testing protocol (once every three days with test performance of 80% sensitivity and 90% specificity).

Table S3. Demographic and clinical summary of patients evaluated by the SARS-CoV-2 Direct Antigen Rapid Test (DART). N response, N or mean of positive, and % or standard deviation for each group is presented. All samples (n=131) collected and tested in São José do Rio Preto, Brazil.

Figure S1. Graphical scheme displaying the relationships between the stages of quarantine and infection in *SIDHRE-Q* model: Q-U, quarantine uninfected; **S**, susceptible (uninfected); **I**, infected undetected (pre-testing and infected); **D**, infected detected (infection diagnosis through testing); **H**, hospitalized (infected with life threatening symptom progression); **R**, recovered

(healed); **E**, extinct (dead); and **Q-R**, quarantine recovered (healed but in quarantine by false positive testing).

Figure S2. COVID-19 Outcomes as a result of Frequent Rapid Testing Protocol with variable test performances using *SIDHRE-Q* Model. The Cumulative Detected Infected, Hospitalized, Deceased, Active Infections, Recovered, and Quarantined are modeled over 105 days (top to bottom) using reported data from 4 global regions: Massachusetts, Los Angeles, New York City, and São José do Rio Preto in Brazil (left to right). The COVID-19 population spread and outcomes are modeled under a Rapid Testing Protocol with variable testing frequencies ranging from 1-21 days between tests, and variable test performances: 90% specificity with 90% sensitivity (A), 70% sensitivity (B), 50% sensitivity (C), and 30% sensitivity (D); and 80% specificity with 90% sensitivity (E), 70% sensitivity (F), 50% sensitivity (G), and 30% sensitivity (H). This protocol is compared to a symptom-based Rapid Testing protocol and a symptom-based qRT-PCR protocol.

Figure S3. Effect of Rapid Testing Protocol under variable testing sensitivities and increasing frequency under the *SIDHRE-Q* Model. The Cumulative Infections, Maximum Simultaneously Hospitalized, and Deceased populations are modeled for Massachusetts, Los Angeles, New York City, and São José do Rio Preto in Brazil. The effect of increasing frequency of testing is modeled for various testing sensitivities (30%-90%) with an 80% specificity.

Figure S4. Effect of County Based Rapid Testing strategy on COVID-19 outcomes in California. This protocol varies testing frequency in accordance to the number of recorded

609 cases; the threshold for number of active infections which, if reached, signals to commence
610 everyday testing, the highest frequency considered. A Rapid Test with a 80% sensitivity and
611 90% sensitivity is used in this deployment strategy. Shown is the total cost per person per day
612 versus the cumulative infections, maximum simultaneously hospitalized, and cumulative deaths
613 with varied thresholds for all of CA is shown. The County Based Rapid Testing strategy is
614 compared to uniform testing, which distributes the same number of total tests used in the county
615 strategy, albeit evenly across each county. The effects of uniform testing are modeled for both a
616 Rapid Testing protocol and a qRT-PCR protocol.
617
618 **Figure S5**. **Time series of the four fitted parameters α, ν, μ, and τ (left to right) for MA, LA,**
619 **NYC, and SJRP (top to bottom).** See Table 2 in the Methods section for an explanation of the
620 parameters. The values are extracted every seven days from data provided by the respective
621 regions. The parameters vary significantly over time and location. Flat points occur during the
622 seven day windows where the parameters are held constant. The fitting procedure is also outlined
623 in the Methods section.
624
625 **Figure S6. Time series of the three fitted pieces of data Cumulative Cases, Daily**
626 **Hospitalized, and Cumulative Deaths (left to right) for each county receiving testing in CA;**
627 Ventura (2A), Stanislaus (2B), Santa Clara (2C), San Joaquin (2D), San Francisco (2E), San
628 Diego (2F), San Bernardino (2G), Sacramento (2H), Orange (2I), Los Angeles (2J), Kern (2K),
629 Fresno (2L), Alameda (2M). The counties included satisfy two requirements: population greater
630 than 1.5% of the total CA population and nonzero total number of deaths at each point in time.
631 The fitting procedure is outlined in the Methods section.

References and Notes

1. Coronavirus Disease (COVID-19) Situation Reports, (available at https://www.who.int/emergencies/diseases/novel-coronavirus-2019/situation-reports).

2. T. F. Menkir, T. Chin, J. A. Hay, E. Surface, P. Martinez de Salazar, C. Buckee, M. J. Mina, K. Khan, A. Watts, M. Lipsitch, R. Niehus, Estimating the number of undetected COVID-19 cases exported internationally from all of China. *medRxiv* (2020), doi:10.1101/2020.03.23.20038331.

3. B. Ivorra, M. R. Ferrández, M. Vela-Pérez, A. M. Ramos, Mathematical modeling of the spread of the coronavirus disease 2019 (COVID-19) taking into account the undetected infections. The case of China. *Commun Nonlinear Sci Numer Simul*, 105303 (2020).

4. M. Salathé, C. L. Althaus, R. Neher, S. Stringhini, E. Hodcroft, J. Fellay, M. Zwahlen, G. Senti, M. Battegay, A. Wilder-Smith, I. Eckerle, M. Egger, N. Low, COVID-19 epidemic in Switzerland: on the importance of testing, contact tracing and isolation. *Swiss Med Wkly*. **150**, w20225 (2020).

5. H. Lau, T. Khosrawipour, P. Kocbach, H. Ichii, J. Bania, V. Khosrawipour, Evaluating the massive underreporting and undertesting of COVID-19 cases in multiple global epicenters. *Pulmonology* (2020), doi:10.1016/j.pulmoe.2020.05.015.

6. J. D. Silverman, N. Hupert, A. D. Washburne, Using influenza surveillance networks to estimate state-specific prevalence of SARS-CoV-2 in the United States. *Science Translational Medicine* (2020), doi:10.1126/scitranslmed.abc1126.

7. D. Böhning, I. Rocchetti, A. Maruotti, H. Holling, Estimating the undetected infections in the Covid-19 outbreak by harnessing capture-recapture methods. *Int. J. Infect. Dis.* **97**, 197–201 (2020).

8. Y. H. Baek, J. Um, K. J. C. Antigua, J.-H. Park, Y. Kim, S. Oh, Y. Kim, W.-S. Choi, S. G. Kim, J. H. Jeong, B. S. Chin, H. D. G. Nicolas, J.-Y. Ahn, K. S. Shin, Y. K. Choi, J.-S. Park, M.-S. Song, Development of a reverse transcription-loop-mediated isothermal amplification as a rapid early-detection method for novel SARS-CoV-2. *Emerg Microbes Infect*. **9**, 998–1007 (2020).

9. L. Leo, Mylab gets commercial approval from ICMR for Covid-19 antigen rapid testing kit. *Livemint* (2020), (available at https://www.livemint.com/news/india/mylab-gets-commercial-approval-from-icmr-for-covid-19-antigen-rapid-testing-kit-11595434040321.html).

10. S. Dey, Coronavirus testing: Rapid antigen tests now make up nearly half of daily checks | India News - Times of India. *The Times of India*, (available at https://timesofindia.indiatimes.com/india/rapid-antigen-tests-now-make-up-nearly-half-of-daily-checks/articleshow/77340459.cms).

11. C. B. F. Vogels, A. F. Brito, A. L. Wyllie, J. R. Fauver, I. M. Ott, C. C. Kalinich, M. E. Petrone, A. Casanovas-Massana, M. Catherine Muenker, A. J. Moore, J. Klein, P. Lu, A. Lu-Culligan, X. Jiang, D. J. Kim, E. Kudo, T. Mao, M. Moriyama, J. E. Oh, A. Park, J. Silva, E. Song, T. Takahashi, M. Taura, M. Tokuyama, A. Venkataraman, O.-E. Weizman, P. Wong, Y. Yang, N. R. Cheemarla, E. B. White, S. Lapidus, R. Earnest, B. Geng, P. Vijayakumar, C. Odio, J. Fournier, S. Bermejo, S. Farhadian, C. S. Dela Cruz, A. Iwasaki, A. I. Ko, M. L. Landry, E. F. Foxman, N. D. Grubaugh, Analytical sensitivity and efficiency comparisons of SARS-CoV-2 RT-qPCR primer-probe sets. *Nat Microbiol* (2020), doi:10.1038/s41564-020-0761-6.

12. D. B. Larremore, B. Wilder, E. Lester, S. Shehata, J. M. Burke, J. A. Hay, M. Tambe, M. J. Mina, R. Parker, Test sensitivity is secondary to frequency and turnaround time for COVID-19 surveillance. *medRxiv* (2020), doi:10.1101/2020.06.22.20136309.

13. Z. Shen, F. Ning, W. Zhou, X. He, C. Lin, D. P. Chin, Z. Zhu, A. Schuchat, Superspreading SARS events, Beijing, 2003. *Emerging Infect. Dis.* **10**, 256–260 (2004).

14. J. S. M. Peiris, C. M. Chu, V. C. C. Cheng, K. S. Chan, I. F. N. Hung, L. L. M. Poon, K. I. Law, B. S. F. Tang, T. Y. W. Hon, C. S. Chan, K. H. Chan, J. S. C. Ng, B. J. Zheng, W. L. Ng, R. W. M. Lai, Y. Guan, K. Y. Yuen, HKU/UCH SARS Study Group, Clinical progression and viral load in a community outbreak of coronavirus-associated SARS pneumonia: a prospective study. *Lancet*. **361**, 1767–1772 (2003).

15. X. He, E. H. Y. Lau, P. Wu, X. Deng, J. Wang, X. Hao, Y. C. Lau, J. Y. Wong, Y. Guan, X. Tan, X. Mo, Y. Chen, B. Liao, W. Chen, F. Hu, Q. Zhang, M. Zhong, Y. Wu, L. Zhao, F. Zhang, B. J. Cowling, F. Li, G. M. Leung, Temporal dynamics in viral shedding and transmissibility of COVID-19. *Nat. Med.* **26**, 672–675 (2020).

16. J. Bullard, K. Dust, D. Funk, J. E. Strong, D. Alexander, L. Garnett, C. Boodman, A. Bello, A. Hedley, Z. Schiffman, K. Doan, N. Bastien, Y. Li, P. G. Van Caeseele, G. Poliquin, Predicting infectious SARS-CoV-2 from diagnostic samples. *Clin. Infect. Dis.* (2020), doi:10.1093/cid/ciaa638.

17. G. Giordano, F. Blanchini, R. Bruno, P. Colaneri, A. Di Filippo, A. Di Matteo, M. Colaneri, Modelling the COVID-19 epidemic and implementation of population-wide interventions in Italy. *Nat. Med.* **26**, 855–860 (2020).

18. S. Choi, M. Ki, Estimating the reproductive number and the outbreak size of COVID-19 in Korea. *Epidemiol Health*. **42**, e2020011 (2020).

19. Y. Y. Wei, Z. Z. Lu, Z. C. Du, Z. J. Zhang, Y. Zhao, S. P. Shen, B. Wang, Y. T. Hao, F. Chen, [Fitting and forecasting the trend of COVID-19 by SEIR(+CAQ) dynamic model]. *Zhonghua Liu Xing Bing Xue Za Zhi*. **41**, 470–475 (2020).

20. Z. Yang, Z. Zeng, K. Wang, S.-S. Wong, W. Liang, M. Zanin, P. Liu, X. Cao, Z. Gao, Z. Mai, J. Liang, X. Liu, S. Li, Y. Li, F. Ye, W. Guan, Y. Yang, F. Li, S. Luo, Y. Xie, B. Liu, Z. Wang, S. Zhang, Y. Wang, N. Zhong, J. He, Modified SEIR and AI prediction of the epidemics trend of COVID-19 in China under public health interventions. *J Thorac Dis*. **12**, 165–174 (2020).

21. S. Cao, P. Feng, P. Shi, [Study on the epidemic development of COVID-19 in Hubei province by a modified SEIR model]. *Zhejiang Da Xue Xue Bao Yi Xue Ban*. **49**, 178–184 (2020).

22. R. Huang, M. Liu, Y. Ding, Spatial-temporal distribution of COVID-19 in China and its prediction: A data-driven modeling analysis. *J Infect Dev Ctries*. **14**, 246–253 (2020).

23. A. Godio, F. Pace, A. Vergnano, SEIR Modeling of the Italian Epidemic of SARS-CoV-2 Using Computational Swarm Intelligence. *Int J Environ Res Public Health*. **17** (2020), doi:10.3390/ijerph17103535.

24. M. Gatto, E. Bertuzzo, L. Mari, S. Miccoli, L. Carraro, R. Casagrandi, A. Rinaldo, Spread and dynamics of the COVID-19 epidemic in Italy: Effects of emergency containment measures. *Proc. Natl. Acad. Sci. U.S.A.* **117**, 10484–10491 (2020).

25. C. Hou, J. Chen, Y. Zhou, L. Hua, J. Yuan, S. He, Y. Guo, S. Zhang, Q. Jia, C. Zhao, J. Zhang, G. Xu, E. Jia, The effectiveness of quarantine of Wuhan city against the Corona Virus Disease 2019 (COVID-19): A well-mixed SEIR model analysis. *J. Med. Virol.* **92**, 841–848 (2020).

26. T. Zhou, Q. Liu, Z. Yang, J. Liao, K. Yang, W. Bai, X. Lu, W. Zhang, Preliminary prediction of the basic reproduction number of the Wuhan novel coronavirus 2019-nCoV. *J Evid Based Med*. **13**, 3–7 (2020).

27. C. Reno, J. Lenzi, A. Navarra, E. Barelli, D. Gori, A. Lanza, R. Valentini, B. Tang, M. P. Fantini, Forecasting COVID-19-Associated Hospitalizations under Different Levels of Social Distancing in Lombardy and Emilia-Romagna, Northern Italy: Results from an Extended SEIR Compartmental Model. *J Clin Med*. **9** (2020), doi:10.3390/jcm9051492.

28. F. Yu, L. Yan, N. Wang, S. Yang, L. Wang, Y. Tang, G. Gao, S. Wang, C. Ma, R. Xie, F. Wang, C. Tan, L. Zhu, Y. Guo, F. Zhang, Quantitative Detection and Viral Load Analysis of SARS-CoV-2 in Infected Patients. *Clin. Infect. Dis.* **71**, 793–798 (2020).

29. S. N. Rao, D. Manissero, V. R. Steele, J. Pareja, A Narrative Systematic Review of the Clinical Utility of Cycle Threshold Values in the Context of COVID-19. *Infect Dis Ther*, 1–14 (2020).

30. J. Alizargar, Risk of reactivation or reinfection of novel coronavirus (COVID-19). *J. Formos. Med. Assoc.* **119**, 1123 (2020).

31. D. Batisse, N. Benech, E. Botelho-Nevers, K. Bouiller, R. Collarino, A. Conrad, L. Gallay, F. Goehringer, M. Gousseff, D. C. Joseph, A. Lemaignen, F.-X. Lescure, B. Levy, M. Mahevas, P. Penot, B. Pozzetto, D. Salmon, D. Slama, N. Vignier, B. Wyplosz, Clinical recurrences of COVID-19 symptoms after recovery: viral relapse, reinfection or inflammatory rebound? *J. Infect.* (2020), doi:10.1016/j.jinf.2020.06.073.

32. W. Deng, L. Bao, J. Liu, C. Xiao, J. Liu, J. Xue, Q. Lv, F. Qi, H. Gao, P. Yu, Y. Xu, Y. Qu, F. Li, Z. Xiang, H. Yu, S. Gong, M. Liu, G. Wang, S. Wang, Z. Song, Y. Liu, W. Zhao, Y. Han, L. Zhao, X. Liu, Q. Wei, C. Qin, Primary exposure to SARS-CoV-2 protects against reinfection in rhesus macaques. *Science* (2020), doi:10.1126/science.abc5343.

729 33. M. Ota, Will we see protection or reinfection in COVID-19? *Nat. Rev. Immunol.* **20**, 351 (2020).

730 34. A. Victor Okhuese, Estimation of the Probability of Reinfection With COVID-19 by the Susceptible-Exposed-
731 Infectious-Removed-Undetectable-Susceptible Model. *JMIR Public Health Surveill*. **6**, e19097 (2020).

732 35. Y. Gu, COVID-19 Projections Using Machine Learning. *COVID-19 Projections Using Machine Learning*,
733 (available at https://covid19-projections.com/).

734 36. D. Stadlbauer, J. Tan, K. Jiang, M. Hernandez, S. Fabre, F. Amanat, C. Teo, G. A. Arunkumar, M. McMahon,
735 J. Jhang, M. Nowak, V. Simon, E. Sordillo, H. van Bakel, F. Krammer, *medRxiv*, in press,
736 doi:10.1101/2020.06.28.20142190.

737 37. A. Goodnough, M. D. Shear, The U.S.'s Slow Start to Coronavirus Testing: A Timeline. *The New York Times*
738 (2020), (available at https://www.nytimes.com/2020/03/28/us/coronavirus-testing-timeline.html).

739 38. M. D. Shear, A. Goodnough, S. Kaplan, S. Fink, K. Thomas, N. Weiland, The Lost Month: How a Failure to
740 Test Blinded the U.S. to Covid-19. *The New York Times* (2020), (available at
741 https://www.nytimes.com/2020/03/28/us/testing-coronavirus-pandemic.html).

742 39. S. Kaplan, K. Thomas, Despite Promises, Testing Delays Leave Americans 'Flying Blind.' *The New York*
743 *Times* (2020), (available at https://www.nytimes.com/2020/04/06/health/coronavirus-testing-us.html).

744 40. W. M. de Souza, L. F. Buss, D. da S. Candido, J.-P. Carrera, S. Li, A. E. Zarebski, R. H. M. Pereira, C. A.
745 Prete, A. A. de Souza-Santos, K. V. Parag, M. C. T. D. Belotti, M. F. Vincenti-Gonzalez, J. Messina, F. C. da
746 Silva Sales, P. dos S. Andrade, V. H. Nascimento, F. Ghilardi, L. Abade, B. Gutierrez, M. U. G. Kraemer, C. K.
747 V. Braga, R. S. Aguiar, N. Alexander, P. Mayaud, O. J. Brady, I. Marcilio, N. Gouveia, G. Li, A. Tami, S. B.
748 de Oliveira, V. B. G. Porto, F. Ganem, W. A. F. de Almeida, F. F. S. T. Fantinato, E. M. Macário, W. K. de
749 Oliveira, M. L. Nogueira, O. G. Pybus, C.-H. Wu, J. Croda, E. C. Sabino, N. R. Faria, Epidemiological and
750 clinical characteristics of the COVID-19 epidemic in Brazil. *Nature Human Behaviour*. **4**, 856–865 (2020).

751 41. S. Mervosh, M. Fernandez, 'It's Like Having No Testing': Coronavirus Test Results Are Still Delayed. *The*
752 *New York Times* (2020), (available at https://www.nytimes.com/2020/08/04/us/virus-testing-delays.html).

753 42. K. Gostic, A. C. Gomez, R. O. Mummah, A. J. Kucharski, J. O. Lloyd-Smith, Estimated effectiveness of
754 symptom and risk screening to prevent the spread of COVID-19. *eLife*. **9**, e55570 (2020).

755 43. T. Zitek, The Appropriate Use of Testing for COVID-19. *West J Emerg Med*. **21**, 470–472 (2020).

756 44. I. Bosch, H. de Puig, M. Hiley, M. Carré-Camps, F. Perdomo-Celis, C. F. Narváez, D. M. Salgado, D.
757 Senthoor, M. O'Grady, E. Phillips, A. Durbin, D. Fandos, H. Miyazaki, C.-W. Yen, M. Gélvez-Ramírez, R. V.
758 Warke, L. S. Ribeiro, M. M. Teixeira, R. P. Almeida, J. E. Muñóz-Medina, J. E. Ludert, M. L. Nogueira, T. E.
759 Colombo, A. C. B. Terzian, P. T. Bozza, A. S. Calheiros, Y. R. Vieira, G. Barbosa-Lima, A. Vizzoni, J.
760 Cerbino-Neto, F. A. Bozza, T. M. L. Souza, M. R. O. Trugilho, A. M. B. de Filippis, P. C. de Sequeira, E. T. A.
761 Marques, T. Magalhaes, F. J. Díaz, B. N. Restrepo, K. Marín, S. Mattar, D. Olson, E. J. Asturias, M. Lucera, M.
762 Singla, G. R. Medigeshi, N. de Bosch, J. Tam, J. Gómez-Márquez, C. Clavet, L. Villar, K. Hamad-Schifferli, L.
763 Gehrke, Rapid antigen tests for dengue virus serotypes and Zika virus in patient serum. *Sci Transl Med*. **9**
764 (2017), doi:10.1126/scitranslmed.aan1589.

765 45. Massachusetts Department of Public Health, COVID-19 Response Reporting. *Mass.gov*, (available at
766 https://www.mass.gov/info-details/covid-19-response-reporting).

767 46. California Department of Public Health, COVID-19 Cases - California Open Data, (available at
768 https://data.ca.gov/dataset/covid-19-cases).

769 47. California Department of Public Health, COVID-19 Hospital Data - California Open Data, (available at
770 https://data.ca.gov/dataset/covid-19-hospital-data).

771 48. Department of Health and Human Hygiene, COVID-19 Daily Counts of Cases, Hospitalizations, and Deaths |
772 NYC Open Data, (available at https://data.cityofnewyork.us/Health/COVID-19-Daily-Counts-of-Cases-
773 Hospitalizations-an/rc75-m7u3).

774 49. Sao Jose do Rio Preto Public Health Office, "COVID-19 Surveillance Data, Sao Jose do Rio Preto" (Sao Jose
775 do Rio Preto Public Health Office, Sao Jose do Rio Preto, Brazil).

50. New York State Government, Daily Hospitalization Summary by Region. *New York Forward*, (available at https://forward.ny.gov/daily-hospitalization-summary-region).

51. Massachusetts General Hospital Institute for Technology Assessment, COVID-19 Simulator - Methodology, (available at https://www.covid19sim.org/images/docs/COVID-19_simulator_methodology_download_20200507.pdf).

52. CDC, Coronavirus Disease 2019 (COVID-19). *Centers for Disease Control and Prevention* (2020), (available at https://www.cdc.gov/coronavirus/2019-ncov/cases-updates/commercial-lab-surveys.html).

53. SciPy.org — SciPy.org, (available at https://www.scipy.org/).

54. NumPy, (available at https://numpy.org/).

55. Non-Linear Least-Squares Minimization and Curve-Fitting for Python — Non-Linear Least-Squares Minimization and Curve-Fitting for Python, (available at https://lmfit.github.io/lmfit-py/).

56. Matplotlib: Python plotting — Matplotlib 3.3.1 documentation, (available at https://matplotlib.org/).

57. Plotly: The front-end for ML and data science models, (available at https://plotly.com/).

Acknowledgments

General: We thank Professor Lee Gehrke for critical reading of the manuscript.

Funding: The study is funded, in part, by a Bill and Melinda Gates Foundation Award (INV-017872) to E25Bio, Inc. EN is funded by Tufts University DISC Seed Grant. MLN is supported by a FAPESP grant (#2020/04836-0) and is a CNPq Research Fellow. AFV is supported by a FAPESP Fellow grant (#18/17647-0). GRFC is supported by a FAPESP

Fellow grant (#20/07419-0). BHGAM is supported by a FAPESP Scholarship (#19/06572-2). The funders had no role in the design of the study; in the collection, analyses, or interpretation of data; in the writing of the manuscript, or in the decision to publish the results.

Author contributions: Conceptualization: BBH. Formal analysis: BN, AB, AR, MB, NS, ARG, AV, GCDS, TMILDS, BHGAM, MMM, GRFC, FQ, AFNR, MLG, ENN, IB, BBH. Funding acquisition: IB, BBH. Investigation: BN, AB, AR, MB, NS, ARG, AV, GCDS, TMILDS, BHGAM, MMM, GRFC, FQ, AFNR, MLG, ENN, IB, BBH. Methodology: BN, AB, AR, MB, NS, ARG, AV, GCDS, TMILDS, BHGAM, MMM, GRFC, FQ, AFNR, MLG, ENN, IB, BBH. Project administration: MLN, IB, BBH. Resources: MLN, IB, BBH. Supervision: MB, MLN, ENN, IB, BBH. Validation: BN, AB, AR, MB, ENN, BBH. Visualization: BN, AB, AR, MB, AV, ENN, BBH. Writing—original draft: AR, BBH. Writing—review and editing: BN, AB, AR, MB, NS, ARG, AV, GCDS, TMILDS, BHGAM, MMM, GRFC, FQ, AFNR, MLG, ENN, IB, BBH.

Competing interests: BN, AB, AR, MB, NS, AG, IB, and BBH are employed by or affiliated with E25Bio Inc. (www.e25bio.com), a company that develops diagnostics for epidemic viruses.

Figures and Tables

TABLES

Table 1. Clinical validation summary for the direct antigen rapid test (DART) for SARS-CoV-2 nucleocapsid protein evaluated using 190 retrospectively collected patient nasal swab specimens.

All Data Summary								
		qRT-PCR (gene average)					95% Confidence Interval	
		+	-	Total	Sensitivity	80.0%	76.1%	83.9%
DART (nucleocapsid protein)	+	80	8	88	Specificity	91.1%	88.2%	94.0%
	-	20	82	102	Positive Predictive Value	90.9%	87.9%	93.9%
	Total	100	90	190	Negative Predictive Value	80.4%	76.6%	84.2%
					Prevalence	52.6%	47.8%	57.5%
					Overall Agreement	85.3%	82.8%	87.8%

Table 2. Clinical validation summary for the SARS-CoV-2 direct antigen rapid test (DART) for SARS-SoC-2 spike glycoprotein evaluated using 121 retrospectively collected patient nasopharyngeal swab specimens.

All Data Summary								
		qRT-PCR (gene average)					95% Confidence Interval	
		+	-	Total	Sensitivity	84.7%	80.6%	88.9%
DART (spike glycoprotein)	+	61	7	68	Specificity	85.7%	80.8%	90.6%
	-	11	42	53	Positive Predictive Value	89.7%	86.2%	93.2%
	Total	72	49	121	Negative Predictive Value	79.2%	73.6%	84.9%
					Prevalence	59.5%	53.9%	65.1%
					Overall Agreement	85.1%	82.0%	88.3%

851 **Table 3. Details of parameter values used for *SIDHRE-Q* Model.**

852

<table>
<tr><td>Parameter</td><td colspan="4">Details & Statistics</td></tr>
<tr><td rowspan="5">α</td><td rowspan="5">$\alpha$is the probability that an interaction between an undetected infected person and an uninfected person results in a new infection, divided by the average number of uninfected people an undetected infected person comes into contact with on a given day. $\alpha$is estimated from the data.</td><td></td><td>Mean</td><td>St. Dev.</td></tr>
<tr><td>MA</td><td>0.088</td><td>0.051</td></tr>
<tr><td>LA</td><td>0.090</td><td>0.034</td></tr>
<tr><td>NYC</td><td>0.067</td><td>0.042</td></tr>
<tr><td>SJRP</td><td>0.121</td><td>0.042</td></tr>
<tr><td>η</td><td colspan="4">$\eta$is the probability that an interaction between an infected person and an uninfected person results in a new infection, divided by the average number of uninfected people a detected infected person comes into contact with on a given day.$\eta = 0.01 \cdot \alpha$
The constant relating η, α accounts for a small but nonzero transmission due to the quarantined (detected) infected population. This value was chosen to be small, assuming a quarantined individual will only infect others with low probability.</td></tr>
<tr><td rowspan="5">ν</td><td rowspan="5">$\nu$is the probability that a symptomatic undetected individual is diagnosed on a given day. $\nu$is estimated from the data. $\nu$is multiplied by sensitivity (assume benchmark sensitivity 100% for PCR, as used when fitting).</td><td></td><td>Mean</td><td>St. Dev.</td></tr>
<tr><td>MA</td><td>0.006</td><td>0.005</td></tr>
<tr><td>LA</td><td>0.011</td><td>0.006</td></tr>
<tr><td>NYC</td><td>0.0056</td><td>0.002</td></tr>
<tr><td>SJRP</td><td>0.015</td><td>0.007</td></tr>
<tr><td>ϵ</td><td colspan="4">ϵ is the probability that an asymptomatic undetected infected individual is diagnosed on a given day. $\epsilon = 0$ while fitting (during PCR symptomatic testing). ϵ =(sensitivity/days between tests) when the rapid testing strategy is activated.</td></tr>
<tr><td>λ</td><td colspan="4">λ is the probability that an undetected infected individual transitions to the recovered state on a given day. λ =</td></tr>
</table>

<table>
<tr><td></td><td colspan="4">$1/14$, or the inverse of average recovery time (51).</td></tr>
<tr><td>μ</td><td>μ is the probability that an infected individual develops severe symptoms on a given day and transitions into the hospitalized state. The flow from D to H is assumed to be independent of the ratio I/D, but comes only from the detected infected population, hence why it is multiplied by $(I+D)/D$. μ is estimated from the data.</td><td></td><td>Mean</td><td>St. Dev.</td></tr>
<tr><td></td><td></td><td>MA</td><td>0.0013</td><td>9.5e-4</td></tr>
<tr><td></td><td></td><td>LA</td><td>0.0016</td><td>2.4e-4</td></tr>
<tr><td></td><td></td><td>NYC</td><td>0.0011</td><td>6.6e-4</td></tr>
<tr><td></td><td></td><td>SJRP</td><td>0.0018</td><td>8.0e-4</td></tr>
<tr><td>ρ</td><td colspan="4">$\rho$is the probability that a detected infected individual transitions to the recovered state on a given day.

$\rho = 1/14$, or the inverse of the average recovery time (51).</td></tr>
<tr><td>σ</td><td colspan="4">$\sigma$is the probability that a hospitalized individual transitions to the recovered state on a given day. $\sigma = 1/11$, or the inverse of the average recovery time for a hospitalized individual (51).</td></tr>
<tr><td>τ</td><td>τ is the probability that a hospitalized individual expires on a given day. τ is estimated from the data.</td><td></td><td>Mean</td><td>St. Dev.</td></tr>
<tr><td></td><td></td><td>MA</td><td>0.034</td><td>0.012</td></tr>
<tr><td></td><td></td><td>LA</td><td>0.016</td><td>0.004</td></tr>
<tr><td></td><td></td><td>NYC</td><td>0.036</td><td>0.034</td></tr>
<tr><td></td><td></td><td>SJRP</td><td>0.032</td><td>0.045</td></tr>
<tr><td>γ</td><td colspan="4">γ is the probability of entering either of the quarantine states on a given day from either the Susceptible or Recovered populations. $\gamma = 0$ while fitting (during PCR symptomatic testing). $\gamma = (1 - \text{specificity}) \times (1/\text{days between tests})$ when the rapid testing strategy is activated.</td></tr>
<tr><td>ψ</td><td colspan="4">$\psi$is the probability that an individual exits quarantine on a given day. $\psi = 1/14$, or the inverse of the quarantine period for fixed length quarantine.</td></tr>
<tr><td>Parameter</td><td colspan="4">Details & Statistics</td></tr>
</table>

α	α is the probability that an interaction between an undetected infected person and an uninfected person results in a new infection, divided by the average number of uninfected people an undetected infected person comes into contact with on a given day. α is estimated from the data.		Mean	St. Dev.
		MA	0.088	0.051
		LA	0.090	0.034
		NYC	0.067	0.042
		SJRP	0.121	0.042
η	η is the probability that an interaction between an infected person and an uninfected person results in a new infection, divided by the average number of uninfected people a detected infected person comes into contact with on a given day. $\eta = 0.01 \cdot \alpha$ The constant relating η, α accounts for a small but nonzero transmission due to the quarantined (detected) infected population. This value was chosen to be small, assuming a quarantined individual will only infect others with low probability.			
ν	ν is the probability that a symptomatic undetected individual is diagnosed on a given day. ν is estimated from the data. ν is multiplied by sensitivity (assume benchmark sensitivity 100% for PCR, as used when fitting).		Mean	St. Dev.
		MA	0.006	0.005
		LA	0.011	0.006
		NYC	0.0056	0.002
		SJRP	0.015	0.007
ϵ	ϵ is the probability that an asymptomatic undetected infected individual is diagnosed on a given day. $\epsilon = 0$ while fitting (during PCR symptomatic testing). $\epsilon =$ (sensitivity/days between tests) when the rapid testing strategy is activated.			
λ	λ is the probability that an undetected infected individual transitions to the recovered state on a given day. $\lambda = 1/14$, or the inverse of average recovery time (*51*).			
μ	μ is the probability that an infected individual develops severe symptoms on a		Mean	St. Dev.
		MA	0.0013	9.5e-4

<table>
<tr><td></td><td>given day and transitions into the hospitalized state. The flow from D to H is assumed to be independent of the ratio I/D, but comes only from the detected infected population, hence why it is multiplied by $(I+D)/D$. μ is estimated from the data.</td><td>LA
NYC
SJRP</td><td>0.0016
0.0011
0.0018</td><td>2.4e-4
6.6e-4
8.0e-4</td></tr>
<tr><td>ρ</td><td colspan="4">ρ is the probability that a detected infected individual transitions to the recovered state on a given day.

$\rho = 1/14$, or the inverse of the average recovery time (51).</td></tr>
<tr><td>σ</td><td colspan="4">σ is the probability that a hospitalized individual transitions to the recovered state on a given day. $\sigma = 1/11$, or the inverse of the average recovery time for a hospitalized individual (51).</td></tr>
<tr><td>τ</td><td>τ is the probability that a hospitalized individual expires on a given day. τ is estimated from the data.</td><td></td><td>Mean</td><td>St. Dev.</td></tr>
<tr><td></td><td></td><td>MA</td><td>0.034</td><td>0.012</td></tr>
<tr><td></td><td></td><td>LA</td><td>0.016</td><td>0.004</td></tr>
<tr><td></td><td></td><td>NYC</td><td>0.036</td><td>0.034</td></tr>
<tr><td></td><td></td><td>SJRP</td><td>0.032</td><td>0.045</td></tr>
<tr><td>γ</td><td colspan="4">γ is the probability of entering either of the quarantine states on a given day from either the Susceptible or Recovered populations. $\gamma = 0$ while fitting (during PCR symptomatic testing). $\gamma = (1 - \text{specificity}) \times (1/\text{days between tests})$ when the rapid testing strategy is activated.</td></tr>
<tr><td>ψ</td><td colspan="4">ψ is the probability that an individual exits quarantine on a given day. $\psi = 1/14$, or the inverse of the quarantine period for fixed length quarantine.</td></tr>
</table>

857 **FIGURES**

858 **Figure 1. Graphical scheme displaying the relationships between the stages of quarantine**
859 **and infection in *SIDHRE-Q* mode**l. **Q-U**, quarantine uninfected; **S**, susceptible (uninfected); **I**,
860 infected undetected (pre-testing and infected); **D**, infected detected (infection diagnosis through
861 testing); **H**, hospitalized (infected with life threatening symptom progression); **R**, recovered
862 (healed); **E**, extinct (dead); and **Q-R**, quarantine recovered (healed but in quarantine by false
863 positive testing).

864

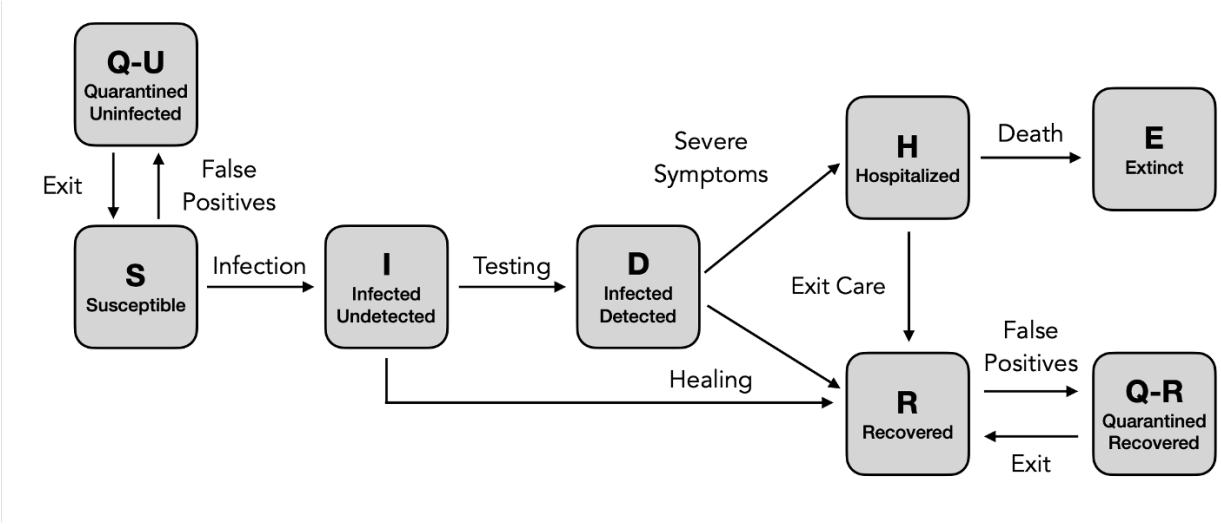

865

866

867

868

869

870

871

872

873

Figure 2. COVID-19 Outcomes in 3 US Regions and Brazil as a result of Frequent Rapid Testing Protocol using the *SIDHRE-Q* Model. (A) The Cumulative Detected Infected, Hospitalized, Deceased, Active Infections, Recovered, and Quarantined are modeled over 105 days (top to bottom) using reported data from 4 global regions: Massachusetts, Los Angeles, New York City, and São José do Rio Preto in Brazil (left to right). The COVID-19 population spread and outcomes are modeled under a Rapid Testing Protocol (sensitivity 80%, specificity 90%) with variable testing frequencies ranging from 1-21 days between tests. This protocol is compared to a symptom-based Rapid Testing protocol and a symptom-based PCR protocol. (B) Effect of Rapid Testing Protocol under variable testing sensitivities (30%-90%) and increasing frequency under the *SIDHRE-Q* Model. The Cumulative Infections, Maximum Simultaneously Hospitalized, and Deceased populations are modeled for Massachusetts, Los Angeles, New York City, and São José do Rio Preto in Brazil with a 90% test specificity.

(A)

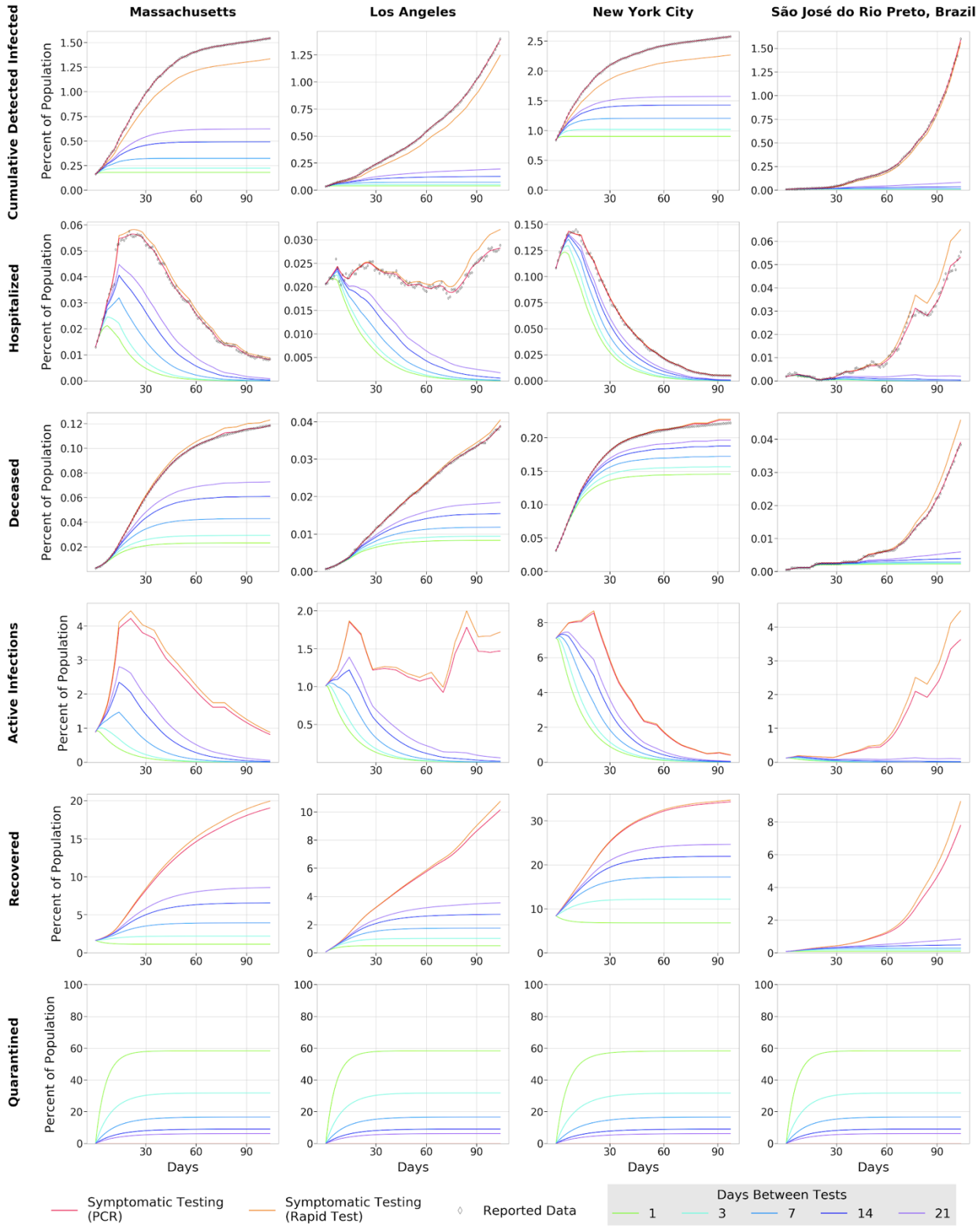

Sensitivity: 80.0% Specificity: 90.0%

(B)

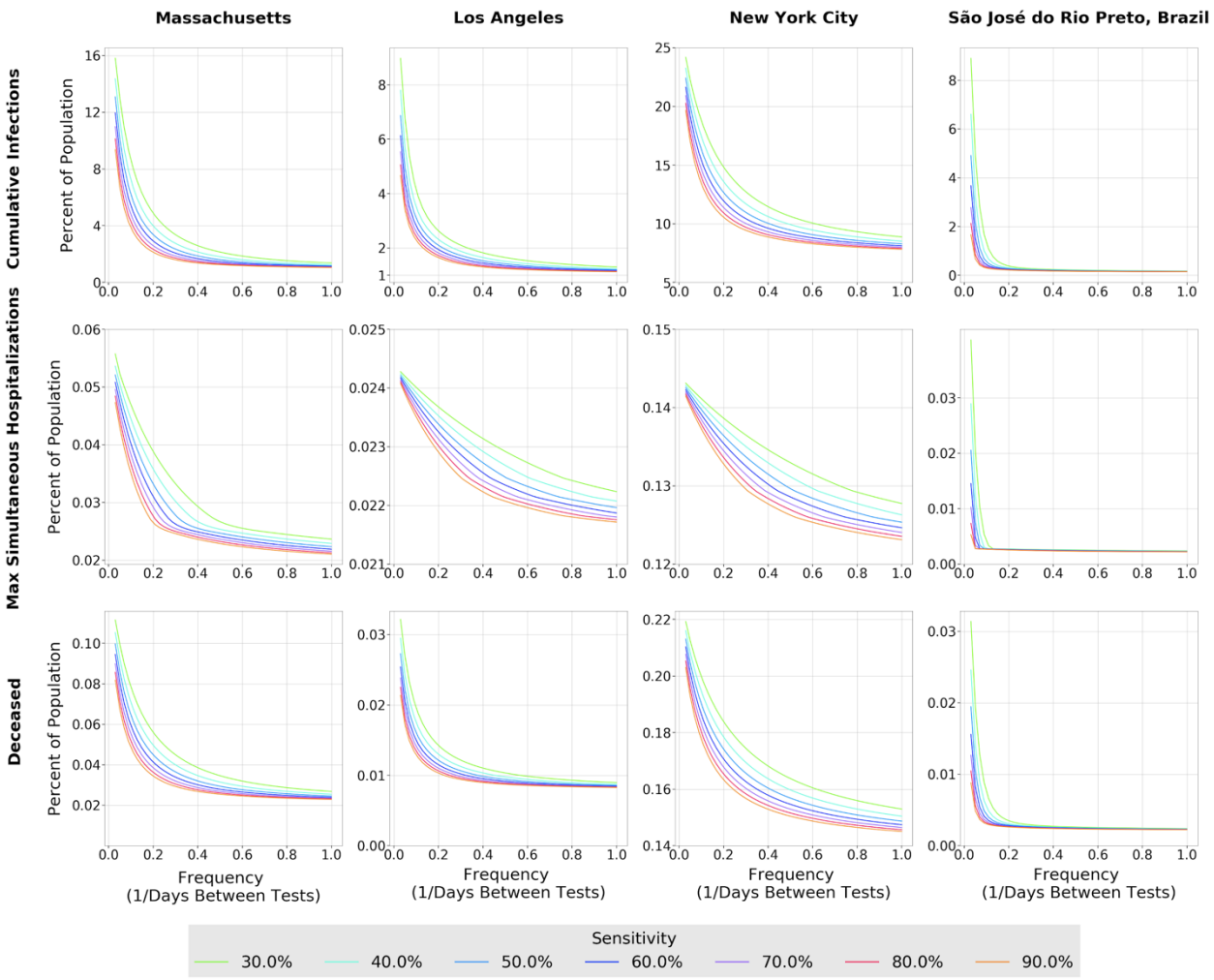

909 **Figure 3. Effect of County Based Rapid Test Protocol (A) and Uniform PCR Protocol (B)**
910 **on active infected detected population over time in California (CA).** The legend denotes the
911 thresholds at which testing frequency is determined, the testing frequencies, the percent of CA
912 population under the strategy, and the cost per person per day.
913
914

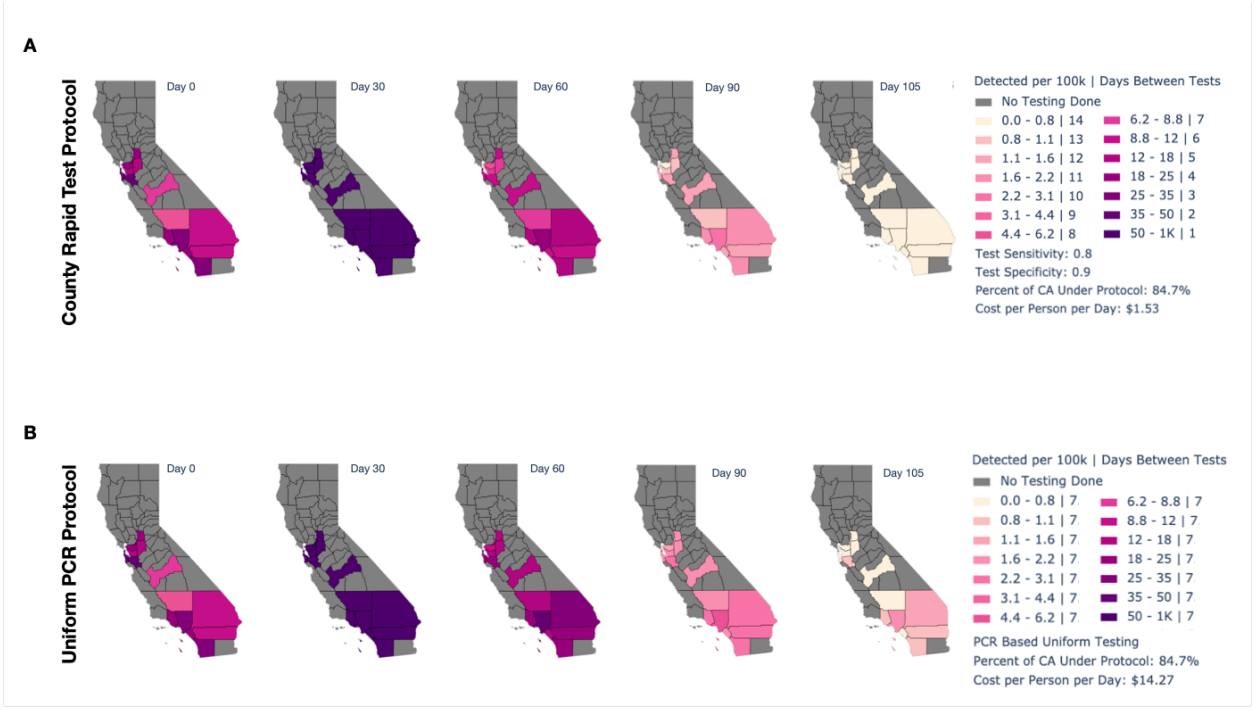

915